Agricultural Biosystems Engineering Group

MSc Thesis Agricultural Biosystems Engineering

Efficient online path planning for weed detection

Tom Lensen

18/10/2023

WAGENINGEN
UNIVERSITY & RESEARCH

Efficient online path planning for weed detection

Name course	:	MSc Thesis Agricultural Biosystems Engineering
Number	:	FTE-82000
Study load	:	36 credits
Date	:	18-10-2023
Student	:	Tom Lensen
Registration number	:	1042233
Study programme	:	MSc Biosystems Engineering
Supervisor(s)	:	Gert Kootstra Rick van Essen
Examiner	:	Ricardo da Silva Torres
Group	:	Agricultural Biosystems Engineering Group Droevendaalsesteeg 1 (Building 107) 6708 PB Wageningen T: +31 (317) 48 29 80 E: office.fte@wur.nl

DISCLAIMER

This report is written by a student of Wageningen University as part of a master programme and is executed under supervision of the chair Agricultural Biosystems Engineering. This report is not an official publication of Wageningen University and research. The content of this report is not the opinion of Wageningen University and Research.

Use of information from this report is for own risk and it is advised to check this independently before the information is used.

Wageningen University is never liable for the consequences that result from use of information from this report.

Wageningen University and Research
Agricultural Biosystems Engineering Group
PO Box 16
6700 AA WAGENINGEN
T: +31 (317) 482980
E: office.fte@wur.nl

Abstract

The world population is estimated to reach 9 billion people by the year 2050. This growing population requires the agricultural production to increase with 70% by 2050. Precision agriculture will play a major role in this increase in production as well as reducing the environmental impact at the same. An important part of precision agriculture is gathering precise information about the farmland. Drones equipped with cameras can, for instance, be used to map farmland and inspect crops or detect weeds. However, drones have a limited range due to their battery capacity, requiring them to efficiently plan a path to scan a field. The objective of this study is to build an adaptive path-planning algorithm that is more efficient than the conventional path-planning methods, such as the lawnmower path, while preserving the same level of accuracy. In this thesis, an adaptive path planning system was built implementing YOLOv7. The flight path of the drone is altered based on the confidence value of the predictions made by convolutional neural network. The newly developed adaptive path planning system and the conventional system were tested in an offline environment. The offline environment consists of two orthomosaic of a field in which the drone flight path was simulated. The flight path of the adaptive path ranged from -22,5% to +10% of the distance of the lawnmower path. The F1-score of the adaptive path ranged from 0.72 to 0.96. The conventional path had a F1-score of 1 at confidence threshold 0.8. The adaptive path can potentially reduce the flying distance. However, reducing the distance also reduces the detection performance.

Keywords: Adaptive path planning, Drone, YOLOv7, Weed detection, Deep learning

Table of contents

1 Introduction

The world population is estimated to reach 9 billion people by the year 2050 (Rosser et al., 2013). The growing population requires the agricultural production to increase with 70% by that same year (Sishodia et al., 2020). This increase in production must be realized whilst the agricultural sector faces severe challenges imposed by climate change, limited arable lands, soil erosion and a limited supply of fresh water. Precision agriculture can be an important part of the solution to these problems. Precision agriculture refers to technologies and applications that result in more precise and efficient farming. Precision means that the correct technique or substance is applied at the correct time and location. The aim of precision agriculture is to increase the yield and at the same time minimize the use of resources (Basiri et al., 2022). An important part of precision farming is to gather information, such as weed density, crop health or nutrient concentration, of a farmland. The information is acquired with sensors that are mounted on tractors, mobile robots or unmanned aerial vehicles (UAV) i.e., drones. The information that is gathered by drones is used to inspect crops for health and disease (Reinecke & Prinsloo, 2017) and to detect weeds (Hasan et al., 2021). Weed detection is a good example of precision agriculture. Knowing the exact location of all the weeds in a field can be used to precisely spray each weed individually instead of spraying the entire field which reduces the use of chemicals. The information can also be used to guide a robot to mechanically remove the weeds. . Drones have many advantages such as high flexibility, are relatively cheap to run, can perform tasks autonomously, can land and take off vertically and they can hover. However, there are also challenges that need to be addressed such as safety, collision avoidance, and most importantly limited battery capacity (Basiri et al., 2022). The development of batteries increasingly improves the capacity and energy density of batteries (TechTimes, 2023). Besides increasing the energy supply, efficient use of the available energy could also be a solution for the energy challenge. Efficient path planning that shortens flight time could be such a solution. This thesis aims to develop and evaluate an adaptive path planning approach that allows a drone to make decisions regarding its path, in flight, using available sensor data.

1.1 Current situation

The current strategy to map a field with a drone is to fly over the field following parallel lines at relatively low altitude, capturing every part of the field in high resolution. The pattern of parallel lines is also referred to as a 'lawnmower' path. The drone can be steered by a pilot on the ground but usually a flight mission is programmed. The drone executes the flight mission autonomously using information about its location from a global position system (GPS). The flight mission specifies the flying height, the overlap of the images and the flying speed. During flight the onboard sensors capture high-resolution images or other data relevant to the mapping objectives. This can include RGB imagery, multispectral or hyperspectral imagery, LiDAR data or thermal imagery. After the flight, the collected data is transferred to a computer for processing. Specialized software is used to process the aerial images, stitching them together to create a high-resolution orthomosaic map. This map provides a detailed and accurate representation of the field, showing features such as vegetation health, weed pressure and topography. This current mapping strategy faces the challenge of planning paths for efficient data gathering considering the constraints of energy and time (Popovic et al., 2017). The distance or time a drone is able to fly depends on, among other factors, its energy consumption, battery capacity and weather conditions. These factors limit the usability of drones for big arable fields and land masses as the batteries of the drone have to be switched out.

1.2 Desired situation

For mapping purposes, where features of interest are uniformly distributed over the field, the current method is very effective. However, for mapping weeds in a field this is not always the case. Weeds are usually not homogeneously spread across the field (Mortensen et al., 2015). Therefore, it is not necessary to map the entire field in high resolution, only the area of a field where the weeds are present. There have already been attempts to address this issue with the use of online path planning (Popovic et al., 2017; Sadat et al., 2015). Online path planning refers to the process of generating a path in real-time for a mobile agent navigating in an unknown or dynamic environment. The trajectory is altered based on information gathered by the sensors of the agent (Raja, 2012).

Implementing online path planning in weed-detecting drones could significantly reduce the time and flight distance needed to map a field compared to the currently used lawnmower style method (Stache et al., 2021). A weed-detection system with online path planning could fly at higher altitude and faster. The system scans the field for areas that might contain weeds and when it finds those areas, the drone will fly at a lower altitude to make a high-resolution image for detection. The drone proceeds its high-altitude flight path after it is finished imaging the area. This approach could reduce the flight distance needed to map a field and extent the range of the drone. This online path planning could also be used in other domains such as search and rescue missions.

1.3 Problem definition

Due to the rapid development of deep learning algorithms, it is now possible to detect and classify weeds fast and accurate enough that it can be integrated in online path planning. The components, online path planning and weed detection using deep learning, have been studied extensively individually (Farooq et al., 2019; Hoang Trong et al., 2020; Popovic et al., 2017; Rückin et al., 2022; Sadat et al., 2015; Stache et al., 2021; Suh et al., 2018; Zhang et al., 2018). However, they have not yet been combined into one system where the path of the drone is redirected in flight to regions of interest detected by the weed detection algorithm.

The predictions of the deep learning algorithm determine the path of the drone. A prediction of an object has a confidence value that tells something about the validity of the prediction. It is not known yet what the optimal threshold is to accept a prediction or when to reject it. This is key knowledge for the system to perform well. The optimal flying altitudes need te be determined because at the low flying altitude the system needs to classify the objects correctly and at the high flying altitude it needs at least be able to detect all the objects.

The entire system will then work as follows: An image is captured that is processed by a deep learning network. The predictions are evaluated and a decision is made, based on the confidence value, to follow the existing path or to change the flying path to take another image that has a higher resolution. After the new image is made and processed the drone will then continue with the existing flying path.

1.4 Objective

The objective of this thesis is to develop and evaluate an adaptive path planning algorithm based on the processing of the current camera image, which is more efficient in terms of flight distance travelled while maintaining the same detection accuracy of the conventional

method. The algorithm should detect objects such as plants and weeds in flight and changes the drone's flight path if needed.

1.5 Research question

This study aims to answer the following research question:

- What is the difference in performance, in terms of flight distance and detection accuracy, between the proposed online path planning method and the conventional lawnmower path planning method for an autonomous flying drone?

There are four sub questions that help answer the main research question. The first sub question provides insight for the design of the online path planning algorithm. The last two sub questions compare the performance of the two systems.

- SQ1: What is the relationship between the precision and recall of the deep learning algorithm and the flying altitude of the drone?
- SQ2 What is the relationship between the confidence threshold and the precision and recall of the lawnmower path and the adaptive path planner?
- SQ3: What is the difference in flight distance required to map a field for the online path planner and the offline lawnmower path?
- SQ4: What is the percentage of correctly detected objects for the adaptive path planner and the lawnmower path planner?

1.6 Demarcation

To answer sub question one, five different heights will be tested ranging from the lowest possible flying height up to 50 meters. Nine different confidence value settings will be tested to answer question two. Sub questions three and four will be answered by comparing the conventional method and the adaptive method that is made for this thesis. Since it is winter at the time of the measurements, there are no fields that have weeds and plants on them that can be used to test and compare the two methods. To simulate plants and weeds in the field, special markers will be used. The focus is on testing the adaptive online flight planner not on detecting weeds and plants.

2 Literature

2.1 Neural network and weed detection

Deep learning models, such as convolutional neural networks (CNNs), have shown remarkable success in various computer vision tasks such as image classification (Guo et al., 2017), object detection (Zhiqiang & Jun, 2017) and image segmentation (Abdalla et al., 2019). CNNs for weed detection have increased in performance the past few years. They have many advantages over the traditionally used machine learning techniques (Hasan et al., 2021). Crops and weeds can look very similar, which can cause problems for traditional machine learning techniques because they rely on features that are designed by experts. CNNs and other deep learning techniques overcome this problem because they are able to extract these features directly from data. The features are extracted from a training set of images with labeled instances. However, these CNNs require a large dataset of labeled data for each class that they detect. A class is an object or living being such as a car, a person or a plant. The number of labeled instances required to detect a class depends on the CNN and type of images used but vary from requiring at least 100 labeled instances up to 1000+ instances (Google Cloud, 2023). In general, more instances per class improves model performance.

Hasan et al. (2021) made an overview of deep learning techniques that have been used for weed detection. They presented a number of papers where a UAV, equipped with a camera, in combination with a CNN was used for weed detection. There are three main tasks that can be distinguished for weed detection: detection and localization of every object in an image and classify these as either plant or weed. A map of the density and the spread of weeds in a field can be constructed from the detections.

There are multiple review papers that test or compare different CNN architectures such as, Alex-Net, VGG-19, GoogLeNet, Resnet-50, Resnet-101, tiny-YOLOv3, YOLOv3 and Faster R-CNN (Bah et al., 2018; Hasan et al., 2021; Jiang et al., 2022; Singh Dhaka et al., 2021). Suh et al. (2018) compared the transfer learning abilities of different well-known CNN models using images of sugar beet and volunteer potato. The performance of the different performances is shown in Table 1 (Suh et al., 2018).

Table 1: The classification performance among six pe-trained deep learning networks was evaluated with 20 and 30 training epochs. The classification performance was averaged over five repetitions and validated with classification accuracy, training time and classification time. Table is from Suh et al., 2018.

	Training 20 epoch			Training 30 epoch		
	Accuracy(%)	Training time (min)	Classifiaction time (s/image)	Accuracy(%)	Training time (min)	Classifiaction time (s/image)
AlexNet	97.9	9.0	0.0038	97.7	15.6	0.0040
VGG-19	98.4	37.4	0.0130	98.7	71.4	0.0124
GoogLeNet	97.0	23.8	0.0033	97.3	36.9	0.0035
ResNet-50	96.2	40.3	0.0072	97.2	69.8	0.0075
ResNet-101	97.5	106.6	0.0118	98.5	162.0	0.0111
Inception-v3	90.8	88.7	0.0088	94.8	133.0	0.0086

Hoang Trong et al. (2020) trained five different CNN models and tested their performance on the Chonnam National University weeds dataset. The results can be seen in Table 2 (Hoang Trong et al., 2020). They then combined the predictions of the different models using Bayesian conditional probability-based method or with priority weights. The combined model prediction (97,31%) was more accurate than the predictions of the individual models.

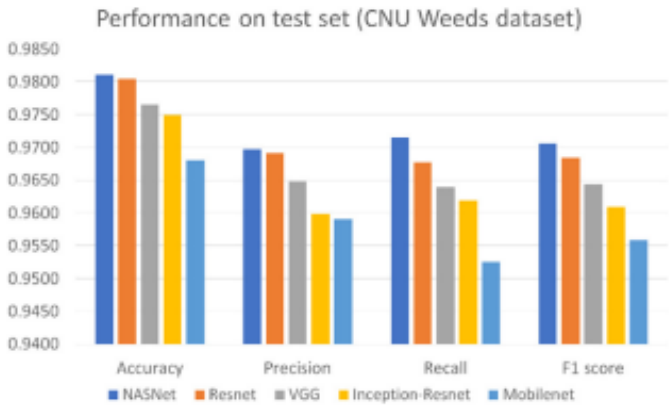

Figure 1: Performance comparison of 5 models on the CNU weeds test set. (Trong et al., 2020)

2.2 YOLO architecture

The power of the YOLO architecture is that it processes the image once to predict objects, hence the name You Only Look Once. That is what makes YOLO very fast as an object detector. Since the first release of YOLO by Redmon et al. (2015), there have been subsequent versions the latest being YOLOv7 at the time of writing. Through the many versions of YOLO the layout of the internal architecture changed each time though the working principal remains the same. An image is divided into $S * S$ grid cells, each grid cells predicts B Bounding boxes along with their positions and dimensions, probability of an object in the underlying grid, and conditional class probabilities. The idea behind detection of an object by any grid cells is that the center of an object should be inside that grid cell. This grid cell is then responsible for detecting that particular object with the help of a bounding box. YOLO predicts parameters for every bounding box. For each grid cell an objectness score is calculated. This objectness score represents the probability that there is an object centered in the grid cell and has a value between 0 and 1 that is calculated by a sigmoid activation function applied to the last convolutional layer. If there is no object in the grid cell the objectness is 0.

A grid cell predicts $B * (5 + n)$ values, where B is the number of bounding boxes and n the number of classes. The tensor shape would be $S * S * B * (5 + n)$. The confidence score is computed for each bounding box per grid by multiplying p_c with Intersection over Union (IoU) between the ground-truth and predicted-bounding-box. If there is no object in the grid cell the confidence score is zero. The next step is to calculate the class specific score (c_{ss}) for each bounding box of all the grid cells. This class specific score is the probability of the class being present in the bounding box and how well the bounding box fits the object. The predicted bounding boxes differ in size to accommodate the different sizes and shapes of objects and are called anchor boxes. An object should be detected by a bounding box that has the center of the object in it. There is a possibility that an object is predicted by multiple bounding boxes. The object is to be predicted by the bounding box that fits the object the best. The others need to be discarded. In order to do that, the bounding boxes that have a class score lower than a set threshold value, usually 0,5, are discarded. After this procedure, we have less bounding boxes but there are still too many. The second step to decrease the number of bounding boxes is called non-maximum suppression (NMS) based on the IoU. The bounding box with the maximum class score is selected and all bounding boxes with an IoU greater than a certain threshold are discarded.

2.3 Path planning algorithms

Over the years path planning algorithms have been developed to fly a drone autonomously from point A to point B efficiently and/or to overcome obstacles between them. Those path planning strategies have been analyzed and categorized by Basiri et al. (2022). They distinguished the following categories: Grid-based, Sampling-based, Artificial Intelligence, Cooperative and Non-cooperative techniques. Almost all of these algorithms are so-called 'offline methods' for path planning. Offline, in this context, means that the path planning is calculated before the drone takes off. The information of the area where the drone flies is known beforehand, the algorithm uses that information to calculate the path. Online methods for path planning calculate and adjust the path whilst the drone is flying based on the information the drone gathers from its surroundings.

2.4 Online path planning

There have been several path planning algorithms that have proposed online path planning strategies. Sadat et al. (2015) made use of the Hilbert curve, a continuous fractal space-filling curve, shown in Figure 3. They placed a grid over the area and set three flying heights for the drone and for each height planned a Hilbert curve path. The drone starts at the highest altitude and detects regions of interest, a grid cell with a frisbee, using a stabilized camera. If a region of interest is detected, the drone drops to a lower altitude to get a better view of the region. The lower altitude path is made of a higher order of the Hilbert curve. Since the Hilbert curve preserves locality (Moon et al., 2001), the drone stays close to its previous location in terms of longitude and latitude.

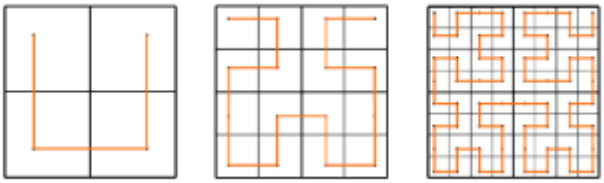

Figure 2: Hilbert curves of first, second and third order (Sadat et al., 2015)

Another online path planning algorithm is proposed by Popovic et al. (2017) with the goal to maximize the information gain with a time budget constraint. The drone had 150 seconds to fly in an area to maximize its information gain. The drone starts at the center of the map at a high altitude where it is able to see the entire area. As it descends down, a series of five viewpoints are chosen using an information objective. This information objective is a set of equations that describe a trade-off between the time cost and the information gained from a certain viewpoint. After each viewpoint, a new viewpoint is chosen, and a path calculated to it as shown in Figure 4.

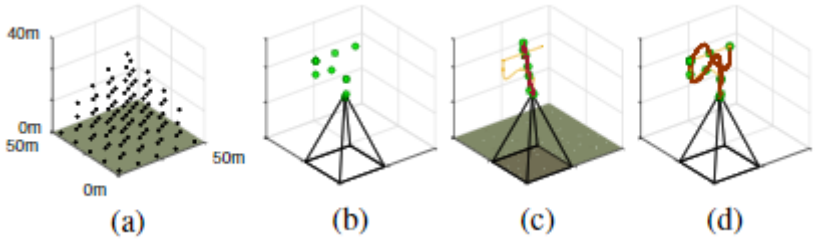

Figure 3: Visualization of viewpoint selection by Popovic et al. (2017) *. First, all possible viewpoints are mapped out (a). Then, a series of viewpoints are selected (b). Whilst flying, the trajectory is adjusted (c) and (d).*

Both these methods of online path planning showed that they are faster than the conventional lawnmower path and they have matching classification performance.

2.5 Factors involving the flying height of a drone

An important aspect of detecting weeds with a drone is the optimal flying altitude. There are a number of factors that influence the ideal flying altitude. First of all, the area that is represented by one pixel is dependent on the altitude of the camera and the resolution of the image. The observable area of the camera is called the field of view (FOV). This factor limits the maximum altitude of the drone because weeds need to be represented at least by a certain number of pixels to be detected. The maximum altitude can be increased by increasing the resolution of the image. However, an image with higher resolution takes longer to process, so there is a maximum to the resolution of the input image. Lam et al. (2021) used three different altitudes (10m, 15m, 20m) to study the effect on the performance of their weed detector, based on the VGG16 architecture, for *Rumex obtusifolius*. They found that the detection accuracy at 10 meters altitude was higher than at 20 meters altitude. The ground sample distance (GSD), the distance between two consecutive pixel centers measured on the ground, was 3 and 6 mm/pixel for . The GSD is calculated by the following formula from Stache et al. (2021),

$$GSD = \frac{h * S_w}{f * I_w}, \qquad \text{[mm/pixel]} \qquad 2.1$$

where h is the altitude of the drone in meters, S_w the sensor width of the camera in mm, f the focal length of the camera in mm and I_w the image width in pixels. A schematic overview of the GSD can be seen in figure 5.

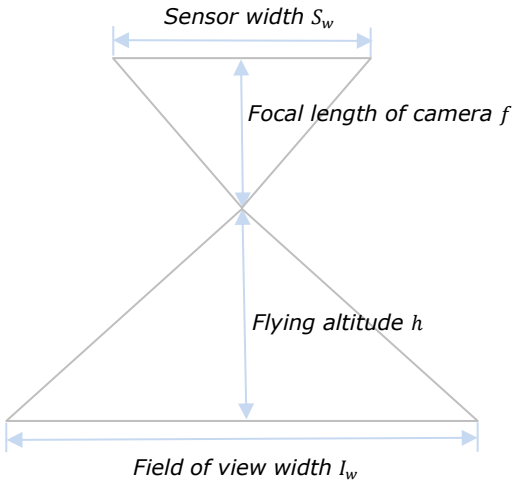

Figure 4: Schematic overview of the elements required to calculate the Ground Sampling Distance (GSD)

The minimal flying altitude is limited by the air displacement of the rotors of the drone. When the drone flies too low, the air displacement will affect and move the plants which makes it impossible to capture useful images.

3 Materials and Methods

3.1 ArUco markers

At the time of collecting images from the field it was winter. Therefore, there were no fields with crops and weeds that could be used. To simulate the presence of weeds and plants in the field, two different Aruco markers were used. The idea to use Aruco markers as substitution for weeds and plants is that these, like plants and weeds, look similar from a distance but can be distinguished from another close up. Aruco markers are square markers with an edge of black pixels and are commonly used for pose estimation (Dimitri van Heesch, 2023). Within this border, there is a matrix of black and white pixels that represents the identity of the marker. The size of the internal matrix is determined by the size of the Aruco marker. A marker with the size 5x5 has an internal matrix of 25 pixels (Dimitri van Heesch, 2023). Two different Aruco markers were used to represent a plant and a weed and are shown in Figure 5. The Aruco markers that were used had a size of 7,5 cm by 7,5 cm. They were printed on A4, cut out and laminated to withstand moisture.

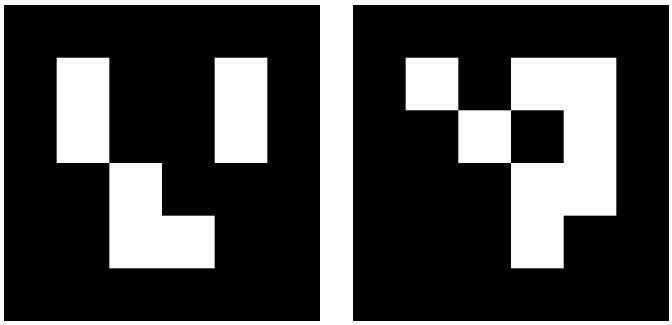

Figure 5: Aruco markers, left is the marker 'weed' and on the right is the marker 'plant'

3.2 Drone and camera

For this thesis, a DJI M300 RTK drone was used (see Figure 6a). This drone is equipped with real time kinematic (RTK) global positioning system (GPS) with a positioning accuracy of 1 cm horizontally and 1,5 cm vertically. The maximum flight time on one set of batteries is 55 minutes depending on the payload (DJI, 2022b). A Zenmuse P1 RGB camera was used to capture images (see Figure 6b). The P1 camera is equipped with a gimbal a 35 mm lens and a field of view angle of 63,5 degrees and makes images with a resolution of 8192x5460 pixels and films in a resolution of 1920x1080 pixels (DJI, 2022a).

Figure 6: DJI Matrice 300 drone (left) and the DJI Zenmuse P1 camera (right) (DJI, 2022a, 2022b)

3.3 Lawnmower path

The image acquisition of the drone was simulated by cutting out pieces with the size of the field of view of the drone from the orthomosaic described in subsection 3.8 at 12 meters altitude. For the lawnmower path, a set of waypoints on the 12 meter altitude orthomosaic was created in such way that the field of view of each point did not overlap with another point. Then, at each waypoint, a piece, the size of the field of view, was cut out of the orthomosaic and processed by the YOLO object detector. The total distance travelled was recorded as well as all the predictions and their confidence score. The schematic overview of the lawnmower path can be seen in Figure 7.

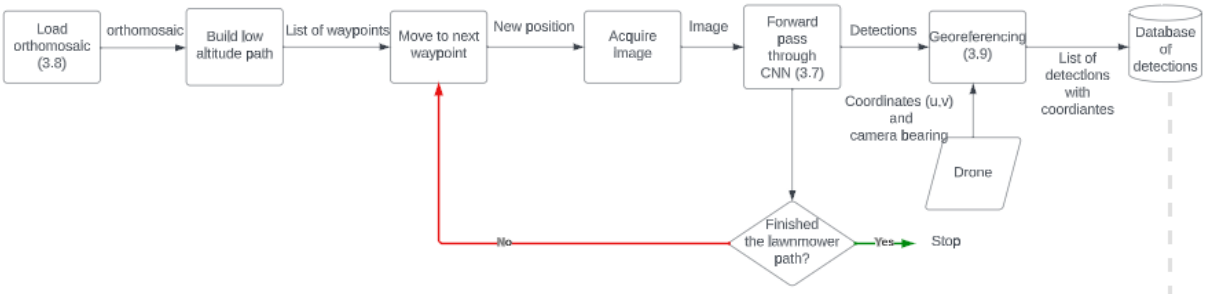

Figure 7: Flowchart of the lawnmower path with references to the explanatory subchapters

3.4 Adaptive path

The adaptive path, as can be seen in Figure 8, had a set of waypoints on the 20 meters altitude orthomosaic. At each waypoint, a piece, the size of the field of view, was cut out from the orthomosaic and processed by the YOLO object detector. Any detections of objects in the image have a confidence value. If that value was between the low threshold value and the high threshold value than that object is in the 'investigation zone' and was marked as an object of interest. All predictions below the low threshold value were ignored and all predictions above the high threshold were accepted. The next step was to determine the position of that object using georeferencing described in section 3.5 and cut out a piece of the 12 meter orthomosaic at that position that is then processed by the object detector.

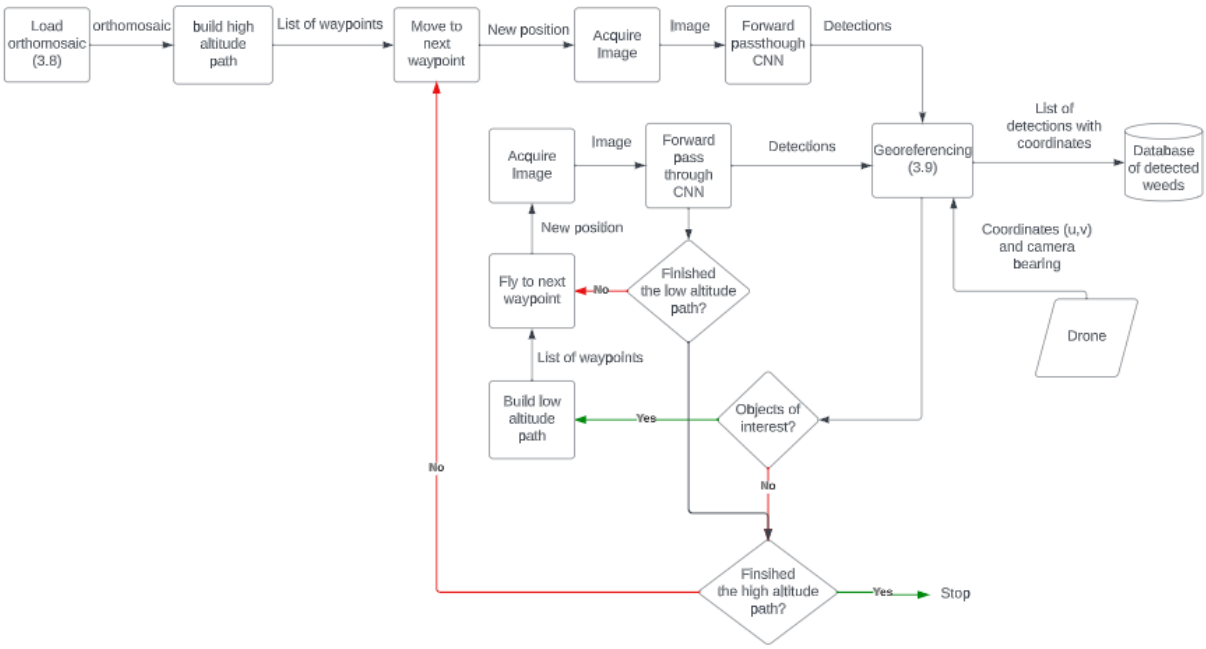

Figure 8: Flowchart of the adaptive path with references to the explanatory subchapters

3.5 Image acquisition

To collect training data for training the object detector, images were made in a field from the Wageningen Unifarm close to the university campus. The location is shown in Figure 9.

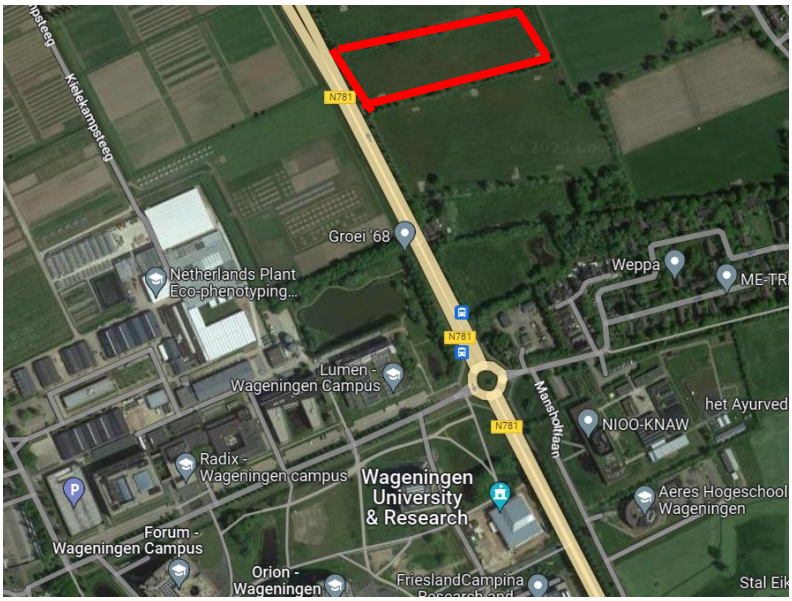

Figure 9: Snippet of Google Maps showing the location of the field, shown with a red rectangle, near the Wageningen university campus

The images were recorded at 18th and 19th of January 2023. On these dates the weather conditions were dry with a maximum wind force of 6-8 km/h. The field has a total area of 1,2 acres. A total of 150 Aruco markers, 75 for each type, were printed and evenly spread out on the field. A lawnmower flight mission was programmed for each of the five flying altitudes. The flying altitudes were 12 meter, 20 meter, 30 meter, 40 meter and 50 meter. During the flight, the camera pointed to the ground surface at an angle of 90 degrees, Table 2 shows the different flying altitudes, the overlap and number of images taken for

each altitude. To decrease the amount of images and reduce flying time, the overlap of the images was changed for the lower altitudes (12m, 20m). The average flying speed of the drone was 1.6 m/s. The drone continued flying as the images were made.

Table 2: Table showing the different flying heights with their overlap and number of images

Altitude [m]	Front overlap	Side overlap	Number of images
12	40%	40%	361
20	40%	40%	132
30	80%	70%	345
40	80%	70%	190
50	80%	70%	116

3.6 Image preprocessing

The resolution of the images was too high and unpractical for training purposes as the batch size would be very low and the processing time would be long. The images were split in 16 images because downsizing the images from a resolution of 8192x5640 to 1920x1280 made the markers unreadable, especially for the images made at higher altitudes. In the experiments the images were also downsized from 8192x5640 to 1920x1280 and larger markers were used. The images containing a marker were used for annotation and training. To make the model more robust, some images without markers were added to the dataset. The images were annotated using Roboflow (Roboflow, 2023). Table 3 shows the number of images for each height and the number of annotated 'plants' and 'weeds'. The images were split in training, validation and test using a 70-20-10 ratio for each altitude. The images for the test set are the images that were taken at the end of the flight mission. This is to prevent that there are markers in the test set that are also in the training set because of overlapping images and affect the test results.

Table 3: Number of training images, validation images, test images, plant objects and weed objects for each flying height

Altitude[m]	Number of Images	Plant objects	Weed objects	Training Images	Validation Images	Test Images
12	242	133	108	170	49	23
20	219	102	114	153	44	22
30	234	108	110	164	47	23
40	212	114	90	149	42	21
50	228	93	135	160	46	22

3.7 Training object detector

The object detector that was used for this thesis is the YOLOv7 architecture from the paper written by Wang et al. (2022) taken from their Github repository [1]. YOLOv7 is one of the latest version of YOLO at the start of this thesis and performs better in terms of speed and accuracy than its predecessors (Wang et al., 2022). The model is trained on a computer with a Nvidia GeForce 1080Ti graphics card. Table 4 shows the parameters that have been changed from the default setting and their corresponding values used for training the model.

[1] https://github.com/WongKinYiu/yolov7

Table 4: Parameters and corresponding values that were used to train the object detector. All other parameters are left at their default value.

Parameter	Value
Batch size	5
image size	1088
Epochs	600

3.8 Offline environment

The adaptive and lawnmower path were tested and compared in an offline environment using actual images of a field with objects. Aruco markers were scattered on the same field that was used in section 3.5 . Two flight missions were planned to take images with 70% front and 80% side overlap at 12 meters and at 20 meters altitude. The images were resized from 8192*5460 to 1920*1280 to decrease calculation time. These images were then stitched together into orthomosaic photos using Agisoft Metashape. Six of the markers were used as ground control points (GCP) to accurately stitch images together.

3.9 Georeferencing

An integral part of the adaptive path planning method is to determine the location of a detected object in the real world. Georeferencing converts the internal coordinate system of an aerial photo image into geographic coordinates. The real world coordinates of an object of interest are calculated using the object location in the image (u, v), the current position of the drone $(latitude, longitude)$, the initial azimuth angle (bearing relative to the north) α_1 and the distance s are calculated using Vincenty's formulae (Vincenty, 1975). The Vincenty formulae are a set of equations that take into account the ellipsoid shape of the earth and calculates the shortest distance between two points called the geodesic distance, see Appendix A for more details. The initial azimuth between the drone and the object is calculated by:

$$\alpha_1 = DH + OA, \qquad [°] \qquad 3.1$$

where DH $[-180,180]$ is the drone heading, offset from true north, in degrees and OA is the object angle in degrees. The object angle is the angle between the position of the object in the image (u, v) and the vertical center line of the image as shown in Figure 10.

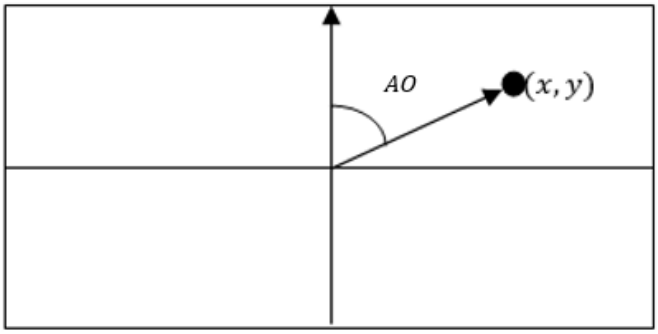

Figure 10: Schematic view of the object angle

The distance is calculated by multiplying the number of pixels between the centre of the image and the object location (u, v) with the ground sampling distance (formula 2.1).

3.10 Performance metrices

The performance of the YOLO object detector was evaluated with the precision and the recall. The network predicts for each grid cell of an image a number of bounding boxes. To filter the predictions, the non-maximum suppression (NMS) technique is applied. This technique removes all bounding boxes that have a confidence value lower than the set threshold. NMS also removes bounding boxes that overlap each other based on the Intersection over Union (IoU) shown in figure 11.

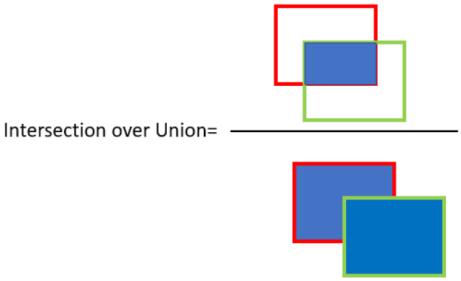

Figure 11: Calculation of Intersection over Union, red is the ground truth bounding box and green is the predicted bounding box(Liuberskis, 2020).

The value of IoU is between 1 and 0, where 1 indicates complete overlap and 0 indicates no overlap. If two bounding boxes have a IoU score greater than the set threshold, the bounding box with the lowest confidence score is removed. The predicted bounding boxes that remain after NMS are used to calculate the precision and the recall. A true positive (TP) is a correctly predicted bounding box and a false positive (FP) is an incorrect prediction of a bounding box. An object that should have been predicted but is not, is a false negative (FN). The precision indicates the number of correctly detected objects out of all the predicted objects in the image and is calculated by:

$$Precision = \frac{TP}{TP+FP} \quad [-] \qquad 3.7$$

The recall is the number of correctly detected objects out of all the objects that are in the image and is calculated by:

$$Recall = \frac{TP}{TP+FN} \quad [-] \qquad 3.8$$

The harmonic mean between the precision and the recall is called the F1 score and is calculated by:

$$F1 = 2 * \frac{Precision*Recall}{Precision+Recall} \quad [-] \qquad 3.9$$

The F1-score is high when both precision and recall are high and is low when either recall or precision is low or both are low.

The accuracy of the georeferencing of the objects is evaluated by comparing the predicted location and the actual location, determined using a RTK GPS receiver, of each object.

Total path length is used to compare the performance of lawnmower and adaptive path. This total distance includes distance travelled vertically for each object that needed investigation for the adaptive path.

3.11 Experiments

3.11.1 Relationship between recall, precision and the flying altitude

To assess the influence of the flying altitude on the precision and recall, the YOLO object detector was tested for five different altitudes. Aruco markers were distributed on a field near the Wageningen campus. Ten images of the field were made at 12, 20, 30, 40 and 50 meters altitude. The resolution of the images were 1920*1080. These images were processed by the object detector and the average precision, recall and F1-score was calculated for each altitude.

3.11.2 Relationship between recall, precision and the confidence value

To investigate the relationship between the confidence score and the precision and recall of the adaptive path, multiple confidence threshold values were used to define an 'investigation zone' that can be seen in Table 5. For each setting, the recall and precision was calculated.

Table 5: The different settings that define the 'investigation zone' of the adaptive path

Setting	1	2	3	4	5	6	7	8	9
Low	0.3	0.3	0.3	0.4	0.4	0.4	0.5	0.5	0.5
High	0.8	0.7	0.6	0.8	0.7	0.6	0.8	0.7	0.6

For the lawnmower path, the precision, recall and F1-score was calculated for ten confidence threshold values between 0 and 1 with interval 0.1. Any prediction with a confidence value higher than the threshold is accepted and predictions below the threshold are ignored.

3.11.3 Flight distance

All waypoints are saved for both the lawnmower path as well as for all the different settings of the adaptive path. The distance between the consecutive waypoints is calculated and added to calculate the total flight distance. The vertical distance of 16 meters was added to the flight distance of the adaptive path for each object that was investigated. The accuracy of the of the georeferencing is calculated by averaging the distance between the ground truth and the predicted position of the markers. This is an average of 40 markers for both the 12 meter orthomosaic and the 20 meter orthomosaic.

3.11.4 Detection accuracy

For both paths, all predictions are saved and counted. For the adaptive path, all objects that needed investigation are saved with the prediction of the 20 meter altitude orthomosaic and the 12 meter altitude orthomosaic.

4 Results

4.1 Relationship between recall, precision and the flying altitude

Figure 12 shows the recall and precision of the object detector at five different altitudes. All the predictions that had a confidence score higher than 0.1 were included. At 12 meters altitude the precision is 100%, all the predictions that have been made are correct. The recall at 12 meter is 90.5 %, meaning not all objects were detected. The higher the altitude, the lower the precision and recall. At 50 meters altitude there have not been any detections and therefore the precision and recall are 0. The precision rapidly declines at altitudes higher than 30 meters. The Recall immediately declines after 12 meters altitude.

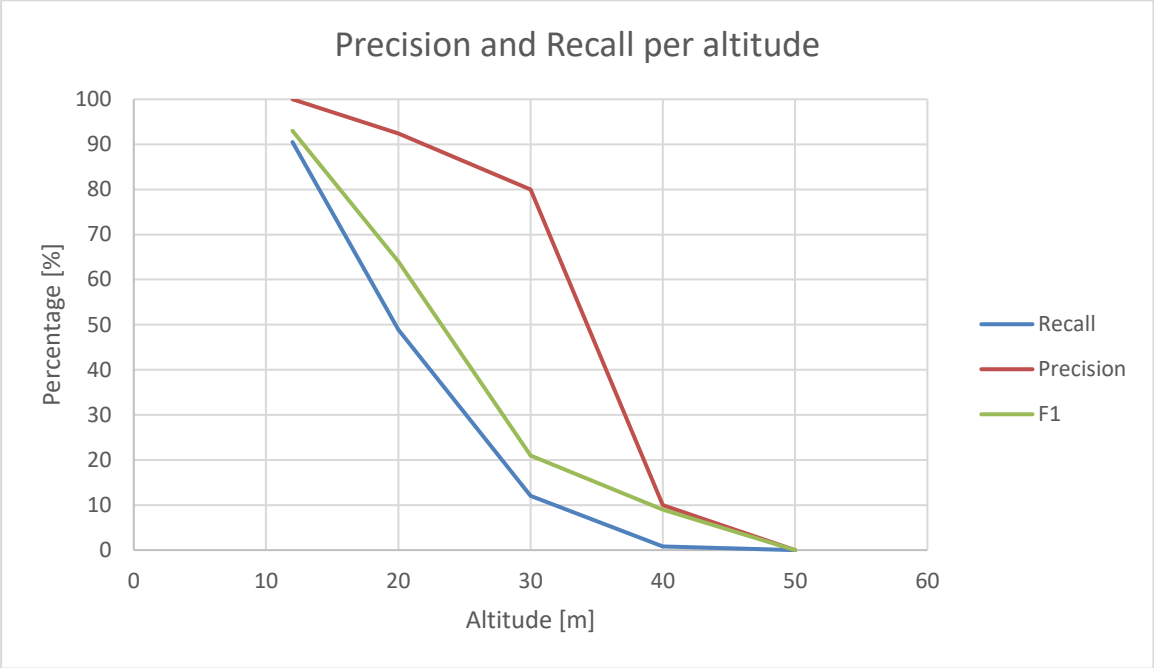

Figure 12:Line chart showing the precision and recall of the object detector at different altitudes

Table 6 shows all the predictions made. Higher altitudes have more detectible objects because more of the field was visible while having the same amount of images. At 20 meters altitude there were three cases of a false positive prediction. These false positive predictions were wrong class predictions.

Table 6 : Table with the all the predictions and the precision and recall for each altitude

Altitude [m]	True positives	False positives	False negative	Precision	Recall	F1
12	31	0	3	100	90.5	0.93
20	38	3	83	92.4	48.9	0.64
30	13	0	94	80	12	0.21
40	1	0	119	10	0.82	0.09
50	0	0	96	0	0	0

4.2 Relationship between recall, precision and the confidence value

Figure 13 shows the precision and recall of the lawnmower path. The optimum confidence threshold is at 0.8. At this threshold, all of the objects are detected and correctly classified without incorrect predictions. The precision increases for increasing confidence threshold values. The recall decreases after a confidence threshold value of 0.8.

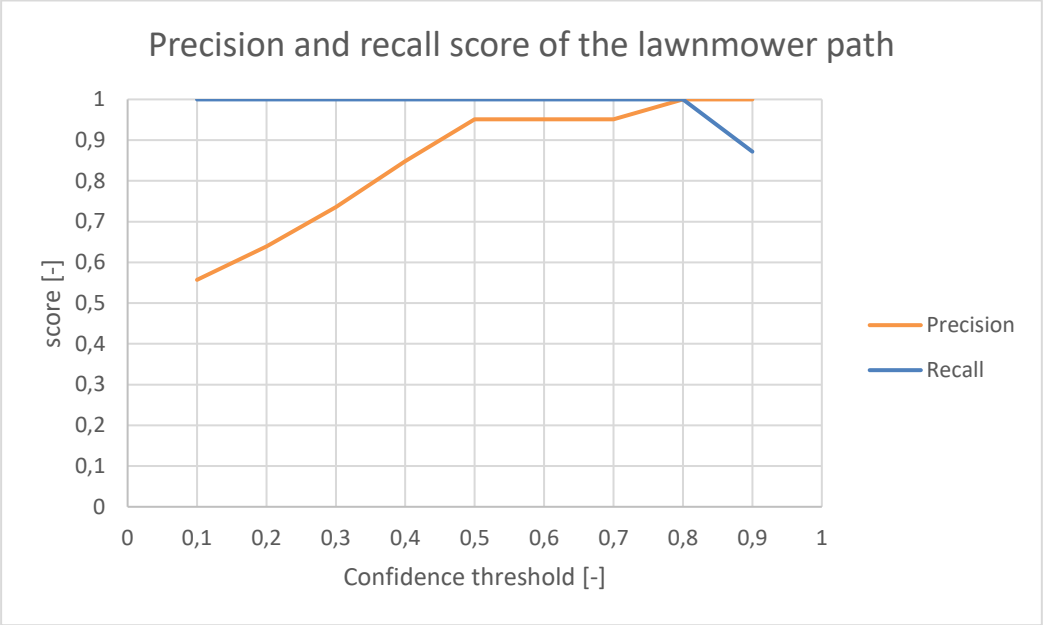

Figure 13: Line chart showing the precision and recall for different confidence threshold values of the lawnmower path

Table 7 shows the recall, precision and F1-score for the different settings of the adaptive path. Setting 1 has the best performance on recall, precision and F1-score. Settings that have a larger discrepancy between the low and high threshold score higher than settings with a smaller discrepancy.

Table 7 : Table with the recall, precision and F1-score for each setting of the adaptive path

	Low threshold	**High threshold**	**Recall**	**Precision**	**F1**
Setting 1	0.3	0.8	0.94	0.98	0.96
Setting 2	0.3	0.7	0.86	0.92	0.89
Setting 3	0.3	0.6	0.78	0.88	0.83
Setting 4	0.4	0.8	0.83	0.98	0.90
Setting 5	0.4	0.7	0.78	0.94	0.85
Setting 6	0.4	0.6	0.67	0.88	0.76
Setting 7	0.5	0.8	0.78	0.98	0.87
Setting 8	0.5	0.7	0.75	0.96	0.84
Setting 9	0.5	0.6	0.61	0.88	0.72
lawnmower	-	0.8	1	1	1

4.3 Flight distance

The flight distance and associated settings of the adaptive path and lawnmower flight distance are shown in Table 8. Settings 3, 5, 6, 8 and 9 have travelled a distance that is smaller than that of the lawnmower path. Setting 1 scores has the highest on precision and recall of all the settings and has the largest travelled distance. Setting 5 and 8 have the highest precision and recall while travelling less distance than the lawnmower path.

Table 8: Table with the travelled distance for each setting of the adaptive path and the lawnmower path

	Low threshold	**High threshold**	**Distance [m]**
Setting 1	0.3	0.8	1342
Setting 2	0.3	0.7	1195
Setting 3	0.3	0.6	1085
Setting 4	0.4	0.8	1245
Setting 5	0.4	0.7	1097
Setting 6	0.4	0.6	985
Setting 7	0.5	0.8	1195
Setting 8	0.5	0.7	1044
Setting 9	0.5	0.6	903
Lawnmower	-	-	1102

The distance between the waypoints at 20 meter altitude without changing the path was 854 meter. The distance of the lawnmower flight path was 1102 meter.

The average distance between the ground truth location and the predicted location was 6 centimetre with a standard deviation of 3.1 centimetre. The distances ranged between 1 centimetre and 10 centimetre.

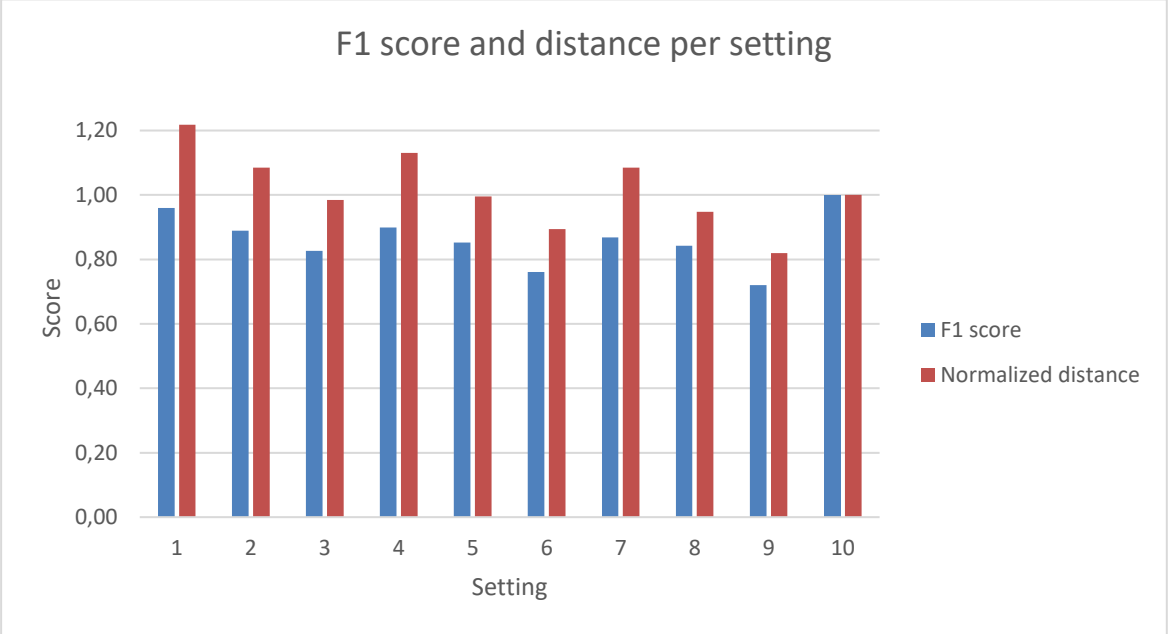

Figure 14: F1 score and normalized travelled distance for each setting of the adaptive path planner, setting number 10 is the lawnmower path

Figure 14 shows the F1 score and the normalized distance of each setting of the adaptive path planner. Setting number 10 is the lawnmower path. The distance is normalized by dividing all distances with the lawnmower path distance. From the figure it can be seen that an increase in distance results in an increase of the F1-score.

4.4 Correctly predicted objects

The lawnmower path correctly predicted all 40 markers at the optimum confidence threshold value of 0.8. Table 9 shows the number of correctly predicted markers for each setting of the adaptive path as well as the number of predictions that were first false and after inspection were correct.

Table 9: The correct and improved number of predictions for all the settings of the adaptive path

	Correctly predicted markers	**Improved predictions**
Setting 1	37	9
Setting 2	34	6
Setting 3	30	4
Setting 4	32	8
Setting 5	30	5
Setting 6	26	3
Setting 7	30	6
Setting 8	29	4
Setting 9	24	1

5 Discussion

There is a negative relationship between the precision and recall of the CNN and the flying altitude. Increasing the flying altitude reduces the precision and the recall. This was expected because the ground sampling distance, the number of millimetres that is represented by one pixel, is lower at higher altitudes when the object and the image size keep the same dimensions.

The images that were used to create Figure 12 and Table 6 were made taking a screenshot from the video feed that was displayed on the remote of the drone. The images contained a lot of blur and this had a negative impact on the performance of the CNN that was trained on images of very good quality. The performance of the CNN on the images used in the offline environment was much better because the images were of better quality. This difference is observed comparing the performance of the CNN from Figure 12 and Figure 13 for the 12 meter altitude where the recall has increased with 10%. Lam et al (2021) found that they had the best detection results of *Rumex obtusifolius* at 10 meters with a GSD of 3 mm/pixel. The images made at 12 meters altitude had a GSD of 6 mm/pixel and the images made at 20 meters altitude have a GSD of 10 mm/pixel. This might suggest that lowering the altitude or increasing the image size increases the performance. Flying at altitudes above 30 meter show little useful results for the adaptive path due to low precision and recall. This can be mitigated by increasing the image size. However, this results in longer processing times that are not favourable for an online adaptive weed detection system that needs to be able to process images fast.

There is a positive relation between the confidence threshold and the precision of the lawnmower path planner. By increasing the confidence threshold, the precision also increases. However, high confidence thresholds will cause the recall to decline because more predictions are filtered out including possible correct detections. There seems to be an optimum confidence threshold score that maximizes both precision and recall. This optimum is calculated by the F1-score. For the lawnmower path, the optimum threshold value can easily be found from Figure 13 and is at 0.8. Both precision and recall and F1-score are 1 meaning that all markers are correctly detected without any false positive detection. This is not realistic in real-world applications. The markers are black and white and have been made to be easily detected.

The relationship between the confidence threshold and the adaptive path planner is the same as for the lawnmower path except for the demarcation of the 'investigation zone'. Determining what predictions need investigation has a big impact on the performance of the adaptive system. A small investigation window, Setting 9, results in a smaller travel distance because less objects need to be visited but comes with a cost of a lower precision and recall. A large investigation window, Setting 1, results in a larger travelled distance with a high precision and recall. Furthermore, defining an investigation zone with relative high threshold values, Setting 7 and 8, results in a higher precision but at a cost of lower recall.

The lawnmower path planner travelled 1102 meters. The length of the waypoints at 20 meters altitude was 854 meter. The adaptive path planner had a travelled distance with a range of 1342 – 903 meter. In general, it can be observed from the results that the setting with the lowest travelled distance also has the lowest precision and recall and that the setting that travelled the longest distance also has the highest precision and recall. This correlation is visible in Figure 14. This can be explained by the fact that an adaptive path

that has travelled a longer distance has seen more objects at a lower altitude and therefore has a higher precision and recall. The altitude difference between the low and high altitude influences the travelled distance for the adaptive path. If there is only one object in an image that needs investigation than the travelled distance is relatively large for a small gain in precision, in comparison to many objects, since the drone needs to fly up and down for only one object. Sadat et al. (2015) divided the flying planes into nodes and if one or more objects were detected in a node, it would visit that node. Depending on the real world application, it might be more efficient to visit nodes instead of individual object locations for example with weeds that tent to cluster. The method that was used in this thesis will perform worse on weeds that are clustered because it will likely fly up and down more because it visits each object individually.

The adaptive path settings have only been tested on one field layout. The markers were spread across the field in such a way that less than 50% of the images cut out from the orthomosaic had markers in them. However, roughly 40% of the images cut out of the orthomosaic contained markers. The performance of the adaptive path in terms of flight distance would increase if the percentage of images with markers would be lower. The orthomosaic could have been altered by deleting markers so that the percentage of images containing markers could have been lower. A layout where all the markers are clustered would likely favor the performance of the adaptive path because the path between individual markers would be shorter than spread out markers.

The adaptive path planner requires some changes and additions to work in a real life agricultural setting. The current offline environment is able to cut-off images discrete from the orthomosaic, this is not possible in a real life application. Overlap of images is required to make sure that every part of the field is included. The overlap of images may have as result that objects are detected multiple times and therefore the system needs to remember earlier detected objects. This problem could be solved with object tracking. If there are objects that need closer inspection and the drone needs to fly to multiple positions it is important that the optimal flight path is calculated. This is a travelling salesman problem where the current position of the drone is the starting point and the next waypoint of the high flying altitude is the end position. A computer with adequate calculation power and electrical power supply are crucial for the system as well as a stable connection between the computer and the drone.

6 Conclusions

The precision of the deep learning algorithm decreases for higher flying altitudes of the drone. The precision at 12 meter altitude was 100% and declined for each increase in altitude. The same is observed with the recall where the recall at 12 meter was 90,5% and decreased for each increase in altitude.

Increasing the value of the confidence threshold, increases the precision and eventually decreases the recall. The performance of the lawnmower path was at an optimum at a confidence threshold of 80%, increasing the confidence threshold decreases the recall. The adaptive path has two confidence thresholds. Increasing the value of the low or high threshold individually will have the same effect as increasing the confidence threshold value for the lawnmower path. Both precision and recall increase for settings that have a larger value range between the low and high confidence threshold.

The adaptive path showed a potential reduction of the required flight distance up to 22,5% compared to the lawnmower path. However, it was also observed that the required flight distance increased with 10% depending on the setting.

The lawnmower was able to detect and correctly predict every object at a confidence level of 80%. The precision of the adaptive path was between 0.88 and 0.98. The recall of the adaptive path was between 0.61 and 0.94.

The answer to the main research question is that the lawnmower path outperformed the adaptive path in terms of precision and recall. The adaptive path, depending on the setting, is able to map the same area while requiring a smaller distance. Travelling a smaller distance comes with a cost of lower precision and recall.

7 Recommendations

Some recommendations for further research can be made from the lessons that were learned while completing this thesis.

The range of different altitudes that was chosen to find the relationship between the altitude and the precision was probably too large. The performance of the object detector at 12 meter, 20 meter and 30 meter flying altitude were promising. However, at 40 meter and 50 meter altitude almost no objects could be detected. For future research it could be interesting to research more flying altitudes between 12 meter and 30 meter. This might increase the efficiency of the system.

The adaptive path planner has been programmed to visit each object individually. The system could be more efficient, especially for fields where objects of interest are clustered, if it would incorporate the node visiting design proposed by Sadat et al. (2015). If there are multiple objects of interest present in a node only one image is necessary, increasing the efficiency of the system.

The number of flying altitudes the drone visits could be increased. If an object of interest is detected it flies to a lower altitude and captures a new image. If the detection is good enough the drone continues its path, if it is not good enough the drone flies down again. This could reduce the distance the drone that the drones flies up and down.

A sensitivity analysis of the effect of the different variables such as the image resolution, flying altitudes, flying speed and processing time on the travelled distance and time. This could give insight of the influence of the different variables and may result in different design choices.

8 Literature

Abdalla, A., Cen, H., Wan, L., Rashid, R., Weng, H., Zhou, W., & He, Y. (2019). Fine-tuning convolutional neural network with transfer learning for semantic segmentation of ground-level oilseed rape images in a field with high weed pressure. *Computers and Electronics in Agriculture*, *167*, 105091. https://doi.org/10.1016/j.compag.2019.105091

Annotation tool. (2023, March 20). Roboflow. https://app.roboflow.com/thesis-2xpmk

Bah, M. D., Hafiane, A., & Canals, R. (2018). Deep Learning with Unsupervised Data Labeling for Weed Detection in Line Crops in UAV Images. *Remote Sensing and Proximal Sensing in Support of Agricultural Cultivation and Crop Risk Management*. https://doi.org/10.3390/rs10111690

Basiri, A., Mariani, V., Silano, G., Aatif, M., Iannelli, L., & Glielmo, L. (2022). A survey on the application of path-planning algorithms for multi-rotor UAVs in precision agriculture. *The Journal of Navigation*, *75*(2), 364–383. https://doi.org/10.1017/S0373463321000825

Dimitri van Heesch. (2023, January 10). *Detection of ArUco Markers*. OpenCV.

DJI. (2022a, November 7). *Zenmuse P1*. DJI Zenmuse P1. https://www.dji.com/nl/zenmuse-p1/specs

DJI. (2022b, December). *DJI Matrice 300 RTK*. DJI Matrice 300M RTK. https://www.dji.com/nl/matrice-300/specs

Farooq, A., Hu, J., & Jia, X. (2019). Analysis of Spectral Bands and Spatial Resolutions for Weed Classification Via Deep Convolutional Neural Network. *IEEE Geoscience and Remote Sensing Letters*, *16*(2), 183–187. https://doi.org/10.1109/LGRS.2018.2869879

Google Cloud. (2023, May 4). *Develop and use ML models*. Https://Cloud.Google.Com/Vertex-Ai/Docs/Image-Data/Object-Detection/Prepare-Data#:~:Text=For%20each%20label%20you%20must,Better%20your%20model%20will%20perform.

Guo, T., Dong, J., Li, H., & Gao, Y. (2017). Simple convolutional neural network on image classification. *2017 IEEE 2nd International Conference on Big Data Analysis (ICBDA)(*, 721–724. https://doi.org/10.1109/ICBDA.2017.8078730

Hasan, A. S. M. M., Sohel, F., Diepeveen, D., Laga, H., & Jones, M. G. K. (2021). A survey of deep learning techniques for weed detection from images. *Computers and Electronics in Agriculture*, *184*. https://doi.org/10.1016/J.COMPAG.2021.106067

Hoang Trong, V., Gwang-hyun, Y., Thanh Vu, D., & Jin-young, K. (2020). Late fusion of multimodal deep neural networks for weeds classification. *Computers and Electronics in Agriculture*, *175*, 105506. https://doi.org/10.1016/j.compag.2020.105506

Jiang, P., Ergu, D., Liu, F., Cai, Y., & Ma, B. (2022). A Review of Yolo Algorithm Developments. *Procedia Computer Science*, *199*, 1066–1073. https://doi.org/10.1016/J.PROCS.2022.01.135

Lam, O. H. Y., Dogotari, M., Prüm, M., Vithlani, H. N., Roers, C., Melville, B., Zimmer, F., & Becker, R. (2021). An open source workflow for weed mapping in native grassland using unmanned aerial vehicle: using Rumex obtusifolius as a case study. *European Journal of Remote Sensing*, *54*(sup1), 71–88. https://doi.org/10.1080/22797254.2020.1793687

Liuberskis, R. (2020, July 15). *Understanding the mAP (mean Average Precision) Evaluation Metric for Object Detection*. Pylessons.Com.

Moon, B., Jagadish, H. V., Faloutsos, C., & Saltz, J. H. (2001). Analysis of the clustering properties of the Hilbert space-filling curve. *IEEE Transactions on Knowledge and Data Engineering*, *13*(1), 124–141. https://doi.org/10.1109/69.908985

Mortensen, D. A., Johnson, G. A., & Young, L. J. (2015). Weed Distribution in Agricultural Fields. In *Soil specific crop management* (pp. 113–124). https://doi.org/10.2134/1993.soilspecificcrop.c9

P. Raja. (2012). Optimal path planning of mobile robots: A review. *International Journal of the Physical Sciences*, *7*(9). https://doi.org/10.5897/IJPS11.1745

Popovic, M., Hitz, G., Nieto, J., Sa, I., Siegwart, R., & Galceran, E. (2017). Online informative path planning for active classification using UAVs. *Proceedings - IEEE International Conference on Robotics and Automation*, 5753–5758. https://doi.org/10.1109/ICRA.2017.7989676

Reinecke, M., & Prinsloo, T. (2017). The influence of drone monitoring on crop health and harvest size. *2017 1st International Conference on Next Generation Computing Applications (NextComp)*, 5–10. https://doi.org/10.1109/NEXTCOMP.2017.8016168

Roser, M., Ritchie, H., Ortiz-Ospina, E., & Rodes-Guirao, L. (2013). *World Population Growth*. OurWorldInData.Org. https://ourworldindata.org/world-population-growth?utm_campaign=Weekly%20newsletter%20of%20Igor%20Chykalov&utm_medium=email&utm_source=Revue%20newsletter

Rückin, J., Jin, L., Magistri, F., Stachniss, C., & Popovi´c, M. P. (2022). *Informative Path Planning for Active Learning in Aerial Semantic Mapping*. https://doi.org/10.48550/arxiv.2203.01652

Sadat, S. A., Wawerla, J., & Vaughan, R. (2015). Fractal trajectories for online non-uniform aerial coverage. *Proceedings - IEEE International Conference on Robotics and Automation*, *2015-June*(June), 2971–2976. https://doi.org/10.1109/ICRA.2015.7139606

Singh Dhaka, V., Vaibhav Meena, S., Rani, G., Sinwar, D., Fazal Ijaz, M., Wo, M., Benzaoui, A., & Jacques, S. (2021). *A Survey of Deep Convolutional Neural Networks Applied for Prediction of Plant Leaf Diseases Academic Editors: Abdeldjalil*. https://doi.org/10.3390/s21144749

Sishodia, R. P., Ray, R. L., & Singh, S. K. (2020). Applications of Remote Sensing in Precision Agriculture: A Review. *Remote Sensing*, *12*(19), 3136. https://doi.org/10.3390/rs12193136

Stache, F., Westheider, J., Marija, F. M., Popovi´c, P., & Stachniss, C. (2021). *Adaptive Path Planning for UAV-based Multi-Resolution Semantic Segmentation*. https://doi.org/10.48550/arxiv.2108.01884

Suh, H. K., IJsselmuiden, J., Hofstee, J. W., & van Henten, E. J. (2018). Transfer learning for the classification of sugar beet and volunteer potato under field conditions. *Biosystems Engineering*, *174*, 50–65. https://doi.org/10.1016/j.biosystemseng.2018.06.017

The future of drones and high-performance batteries. (2023, May 13). Tech Times.

Vincenty, T. (1975). DIRECT AND INVERSE SOLUTIONS OF GEODESICS ON THE ELLIPSOID WITH APPLICATION OF NESTED EQUATIONS. *Http://Dx.Doi.Org/10.1179/Sre.1975.23.176.88*, *23*(176), 88–93. https://doi.org/10.1179/SRE.1975.23.176.88

Wang, C.-Y., Bochkovskiy, A., & Liao, H.-Y. M. (2022). *YOLOv7: Trainable bag-of-freebies sets new state-of-the-art for real-time object detectors*. http://arxiv.org/abs/2207.02696

Zhang, R., Wang, C., Hu, X., Liu, Y., Chen, S., & Su, B. (2018). Weed location and recognition based on UAV imaging and deep learning. *International Journal of Precision Agricultural Aviation*, *1*(1), 23–29. https://doi.org/10.33440/j.ijpaa.20200301.63

Zhiqiang, W., & Jun, L. (2017). A review of object detection based on convolutional neural network. *2017 36th Chinese Control Conference (CCC)*, 11104–11109. https://doi.org/10.23919/ChiCC.2017.8029130

Appendix

A: Vincenty's formulae

Table 2: symbols and their definition from the paper of T. Vincenty (1975)

Symbol	Explanation
a, b	$major\ and\ minor\ semiaxis\ of\ ellipsoid$
f	$flattening = (a-b)/a$
$\emptyset$	$geodetic\ latitude, poistive\ norrth\ of\ the\ equator$
L	$difference\ in\ longitude, positive\ east$
s	$length\ of\ the\ geodesic$
α_1, α_2	$azimuths\ of\ the\ geodesic$
α	$azimuth\ of\ the\ geodesic\ at\ the\ equator$
u^2	$= cos^2\alpha(a^2-b^2)/b^2$
U	$reduced\ latitude, defined\ by \tan U = (1-f)\tan\emptyset$
λ	$difference\ in\ longitude\ on\ an\ auxiliary\ sphere$
σ	$angular\ distance\ P_1, P_2\ on\ the\ sphere$
σ_1	$angular\ distance\ on\ the\ sphere\ from\ the\ equator$
σ_m	$angular\ distance\ on\ the\ sphere\ from\ the\ equator\ to\ the\ midpoint\ of\ the\ line$

$$\tan\sigma_1 = \tan U_1/\cos\alpha_1. \tag{1}$$

$$\sin\alpha = \cos U_1 \sin\alpha_1. \tag{2}$$

$$A = 1 + \frac{u^2}{16384}\{4096 + u^2[-768 + u^2(320 - 175u^2)]\}. \tag{3}$$

$$B = \frac{u^2}{1024}\{256 + u^2[-128 + u^2(74 - 47u^2)]\}. \tag{4}$$

$$2\sigma_m = 2\sigma_1 + \sigma. \tag{5}$$

$$\Delta\sigma = B\sin\sigma\{\cos 2\sigma_m + \tfrac{1}{4}B[\cos\sigma(-1+2\cos^2 2\sigma_m) - \tfrac{1}{6}B\cos 2\sigma_m(-3+4\sin^2\sigma)(-3+4\cos^2 2\sigma_m)]\}. \tag{6}$$

$$\sigma = \frac{s}{bA} + \Delta\sigma. \tag{7}$$

Eq. (5), (6), and (7) are iterated until there is a negligible change in σ. The first approximation of σ is the first term of (7).

$$\tan\phi_2 = \frac{\sin U_1\cos\sigma + \cos U_1\sin\sigma\cos\alpha_1}{(1-f)[\sin^2\alpha + (\sin U_1\sin\sigma - \cos U_1\cos\sigma\cos\alpha_1)^2]^{\frac{1}{2}}}. \tag{8}$$

$$\tan\lambda = \frac{\sin\sigma\sin\alpha_1}{\cos U_1\cos\sigma - \sin U_1\sin\sigma\cos\alpha_1}. \tag{9}$$

$$C = \frac{f}{16}\cos^2\alpha[4 + f(4 - 3\cos^2\alpha)]. \tag{10}$$

$$L = \lambda - (1-C)f \sin\alpha\{\sigma + C \sin\sigma[\cos 2\sigma_m + C \cos\sigma(-1+2\cos^2 2\sigma_m)]\}. \quad (11)$$

$$\tan\alpha_2 = \frac{\sin\alpha}{-\sin U_1 \sin\sigma + \cos U_1 \cos\sigma \cos\alpha_1}. \quad (12)$$

If the terms in u^8 and B^3 are omitted, $\Delta\sigma$ will give a maximum error of less than 0·00005″. Therefore the following simplified equations may be used for lesser accuracy:

$$A = 1 + \frac{u^2}{256}[64 + u^2(-12+5u^2)]. \quad (3a)$$

$$B = \frac{u^2}{512}[128 + u^2(-64+37u^2)]. \quad (4a)$$

$$\Delta\sigma = B \sin\sigma[\cos 2\sigma_m + \tfrac{1}{4}B \cos\sigma(-1+2\cos^2 2\sigma_m)]. \quad (6a)$$